Mathematical Models of Wound Healing: Exploring Diffusion, Chemotaxis, and Cell-Cell Adhesion

Adriana González-Bueno, Margherita Tonon

May 2025

1 Introduction and Biological Background

Wound healing is a highly complex process that consists of overlapping phases and events that work to construct a new functioning tissue. Many mathematical models to describe these events exist, with the purpose of gaining an understanding of the overall process of wound healing.

Wound healing consists of four main stages. The first stage is hemostasis, where a clot of fibrin and other components forms around the wound. A preliminary matrix is formed for healing. Secondly, inflammation occurs: white blood cells arrive at the wound to disinfect the site [1]. During this stage, the damaged tissue releases various chemicals, including cytokines, growth factors, and chemokines. These establish a chemical gradient that peaks at the center of the wound, enabling other cells to travel to the wound space to promote healing [2]. The third stage is proliferation, where fibroblast cells, which are specialized cells that create proteins to provide support to tissues during repair, move into the wound and produce collagen to replace the temporary structure [1]. One of the key ideas behind wound healing is cell migration and division that occurs at this stage. When a wound opens, cells such as fibroblasts and keratinocytes migrate into the wound in response to chemical signals, and begin to divide [3]. As cells replicate at the wound site, we observe the wound closing, as seen in Figure 1. Lastly, collagen helps seal the wound completely; this is known as remodeling [1].

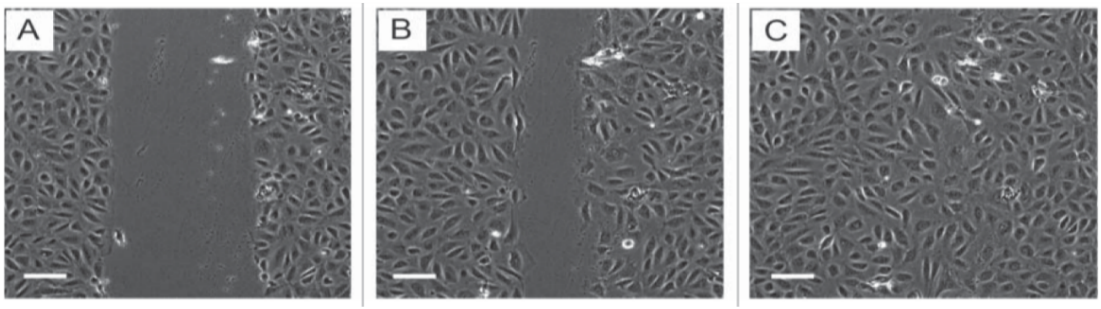

Figure 1: Images of a wound healing in a human vein. Snapshots taken 15 minutes apart. [1]

Many mathematical models have been proposed to describe wound healing. Given the intricate nature of this process, models often isolate individual mechanisms rather than focusing on the entirety of wound healing process as a whole.

This paper aims to explore a few of these models, namely the Fisher Kolmogoroff-Petrovsky-Pisconouff model, the Keller-Segel model, and a model focusing on cell-cell adhesion. We will numerically simulate each model, not only to gain insight into what the wound healing process is like, but also to investigate the nature and effectiveness of these mathematical models in representing a very complex biological process.

2 Fisher-KPP Model

One very simplistic model of wound healing is the Fisher Kolmogoroff-Petrovsky-Pisconouff (Fisher-KPP) model.

The Fisher-KPP model is a semilinear parabolic partial differential equation. Equations of such type give useful insight into the temporal and spatial changes of populations that undergo scattering (movement), spreading (expanding cell surface), and proliferation; these three processes are all present in wound healing, making the Fisher-KPP model a suitable model for providing a simplistic description of how cells (like fibroblasts) spread and grow into a wound space.

The Fisher-KPP equation is defined as:

$$\frac{\partial n}{\partial t} = D\Delta n + rn(1-n) \tag{1}$$

where n represents the cell density, $n \in [0, 1]$. $n = 0$ indicates there are no cells present, and $n = 1$ indicates the cell population has reached its maximum carrying capacity. The term Δn is the Laplacian operator, which in one-dimensional Cartesian coordinates is defined as $\Delta n = \frac{\partial^2 n}{\partial x^2}$. This term represents diffusion, modeling random movement of cells. $D > 0$ is the diffusion coefficient, determining the strength of the diffusion. $rn(1-n)$ is a simple logistic growth equation with carrying capacity 1, as 1 is the maximum cell density, and linear growth rate r. This equation has a stable solution of $n = 1$ everywhere, indicating that the wound has healed.

This model is useful in understanding the initial stages of healing when cells are spreading to close the wound and growing by replicating via mitosis.

We numerically simulated this equation by considering a rectangular domain Ω, representing a bird's eye view of the wound. For the initial condition, we assume that the monolayer is at confluence except for at the wound area – essentially, we binarize the monolayer such that the cell density is 0 at the wound and 1 everywhere else. We consider Neumann boundary conditions on all four sides of the domain, essentially not allowing cells to enter or exit the wound domain [4].

To numerically simulate these, we begin by discretizing the domain. We consider a rectangular region $N = 100$ by 100 pixels, with spatial step dx. The model evolves in pixels over time. The diffusion coefficient D is measured in pixels^2 per unit of time, whereas r has units $\frac{1}{\text{time}}$. Habbal et al. state that 1 pixel is roughly equivalent to 26.6 μm (micrometers); our 100 by 100 pixel domain therefore represents a region of roughly 2.66 by 2.66 mm (millimeters). They define r to range between 10^{-6} and 0.5, and D to range between 10^{-8} and 0.15 [4].

We numerically compute the Laplacian using a five-point stencil, and use Explicit Euler's method in order to numerically simulate the PDEs progressing over time.

We firstly analyze the influence that r has on the healing process. Figure 2 shows snapshots at $t = 1, 10, 50, 100, 150$, and $t = 200$ of the process of a wound healing.

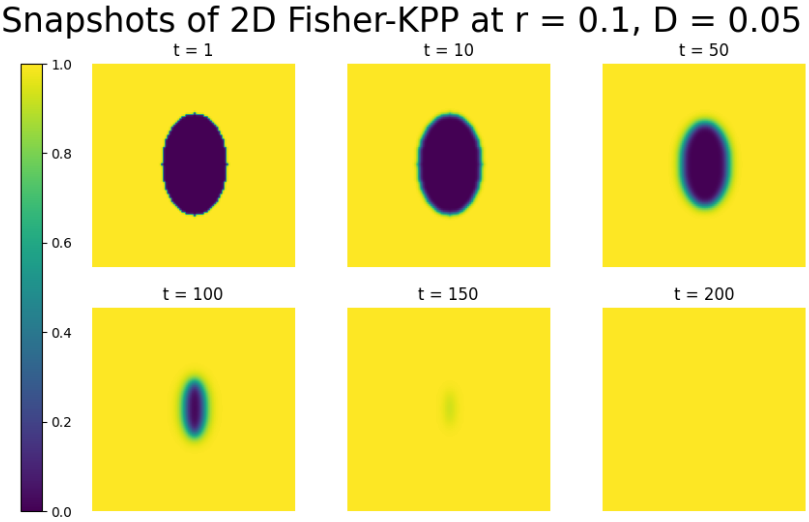

Figure 2: Snapshots of an oval wound healing over time, with $r = 0.01$ and $D = 0.05$. The purple areas represent cell density $n = 0$ while the yellow areas represent cell density $n = 1$.

At $t = 0$, we have an oval-shaped wound, with cell density $n = 0$ inside of it and cell density $n = 1$ outside. We clearly see that at time $t = 200$, the wound has healed as the cell density is 1 across the entire domain.

As seen in Figure 3, increasing r speeds up the healing process, and by time $t = 100$, the wound has already fully healed.

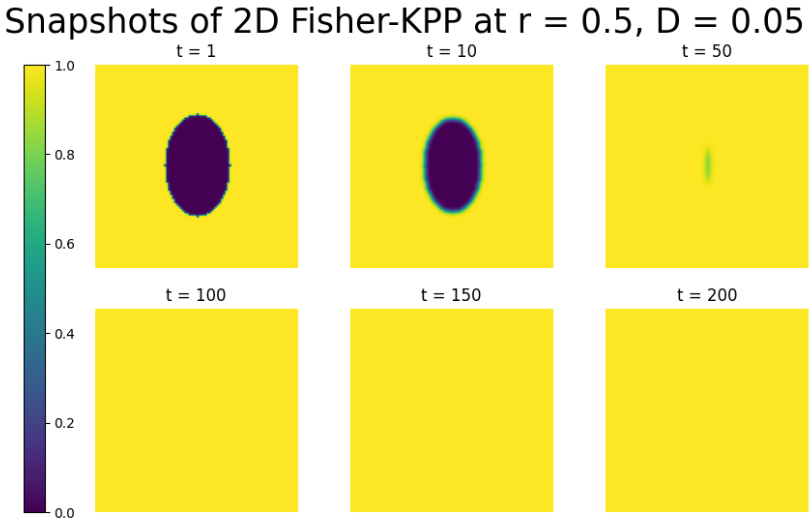

Figure 3: Snapshots of an oval wound healing over time, with $r = 0.5$ and $D = 0.05$.

Increasing r increases the growth rate of the cells entering the wound; therefore, it makes sense that the wound closes more quickly as cells duplicate faster to fill it. When we decrease r, we expect to see the opposite effect – the wound heals slower (Figure 4).

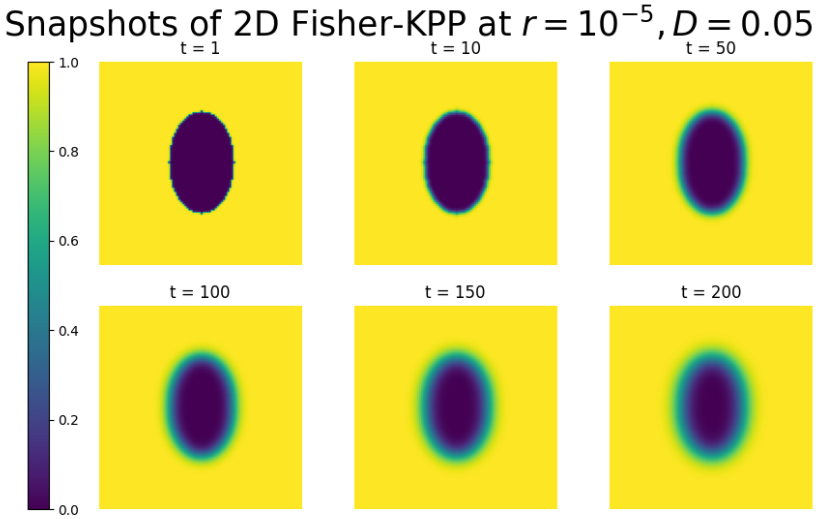

Figure 4: Snapshots of an oval wound healing over time, with $r = 0.00001$ and $D = 0.05$. At $t = 200$, the wound is yet to heal.

Figure 4 highlights the need for a sufficiently high growth rate. The growth rate $r = 0.00001$ was significantly lower than the diffusion coefficient $D = 0.05$; cells were spreading out faster than they were replicating. One potential long-term behaviour of the system is that the wound remains open – cells do not proliferate fast enough to fill the gap, causing the wound to not heal.

D is the diffusion coefficient; as D increases, for a sufficiently large value of r we expect to see the wound heal faster as cells spread more rapidly. This is observed in Figure 5, where at $t = 150$

the wound has healed.

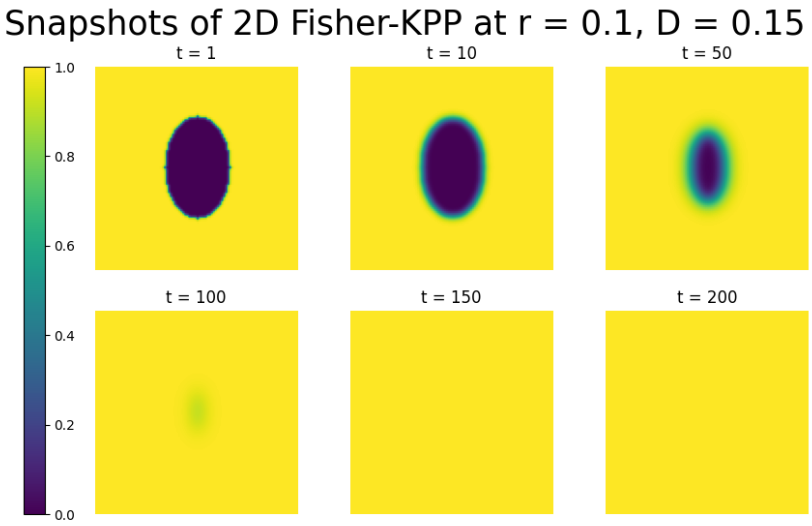

Figure 5: Snapshots of an oval wound healing over time, with $r = 0.1$ and $D = 0.15$.

Increasing the diffusion coefficient therefore has a similar effect to increasing the growth rate, in that both decrease the time it takes for the wound to heal. When we increase the growth rate, we promote proliferation of cells, which consequently increases the cell density. The elevated density pushes the cells to diffuse towards the wound faster. However, when we increase the diffusion coefficient, we "allow" cells to spread faster over the wound, but their growth rate does not increase. As a result, the edges of the wound appear fuzzier or more diffusive: cells move into the wound faster than they replicate, leading to a smoother visual effect rather than a sharper edge.

In Figure 6, we compare a wound with growth rate $r = 0.1$ and diffusion coefficient $D = 0.15$ (left) to a wound with growth rate $r = 0.15$ and diffusion coefficient $D = 0.05$ (right) at $t = 50$. We can clearly see how the wound with higher diffusion coefficient and lower growth rate has fuzzier edges, as cells spread faster than they replicate. On the other hand, the wound with lower diffusion coefficient but higher growth rate has a sharper edge, since cells replicate fast enough to maintain cell density as they spread.

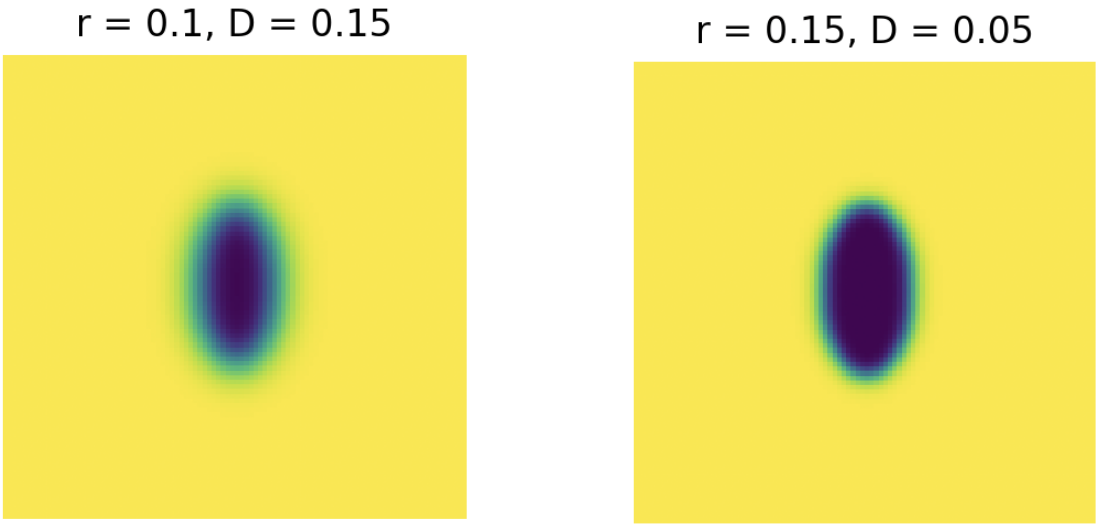

Figure 6: Snapshots of two wounds with different r and D parameter values at $t = 50$.

3 Chemotaxis

While the Fisher-KPP model gives an intuitive overview of the wound healing process, many biochemical factors are neglected. One such factor is chemotaxis – when cells exhibit directed movement in response to chemical cues. In the inflammation stage of wound healing, certain chemicals, such as cytokines and chemokines, provide a gradient for other cells to arrive at the wound space. Therefore, a more realistic model would be one which takes into account the influence of this chemical gradient.

The Keller-Segel model is an extension of the Fisher-KPP model which includes the chemotaxis term, therefore becoming a system of partial differential equations taking into account both the cell density n and chemoattractant concentration c (Equation 2).

$$\begin{aligned} \frac{\partial n}{\partial t} &= D\frac{\partial^2 n}{\partial x^2} - \alpha\frac{\partial}{\partial x}\left(\frac{n}{c}\frac{\partial c}{\partial x}\right) + f(n) \\ \frac{\partial c}{\partial t} &= -\kappa n \end{aligned} \tag{2}$$

Here, D is the diffusion coefficient, and $f(n)$ represents cellular proliferation. We take $f(n)$ to be $rn(1-n)$ where r is a parameter representing the linear growth rate [5].

The chemotaxis term is represented by $-\alpha\frac{\partial}{\partial x}\left(\frac{n}{c}\frac{\partial c}{\partial x}\right)$. $\frac{\partial c}{\partial x}$ is the gradient of the chemoattractant, or how much its concentration changes over space. $\frac{n}{c}\frac{\partial c}{\partial x}$ models the chemotactic sensitivity of cells. Some cells, such as fibroblasts, are capable of detecting extremely shallow gradients. In wound healing, this means that cells can begin moving towards the wound as soon as the chemical is released, despite the concentration being low [6]. When c is small, $\frac{n}{c}$ increases; this term therefore models how cells detect relative changes in chemicals more than they detect absolute amounts. Taking the partial derivative of this, $\frac{\partial}{\partial x}\left(\frac{n}{c}\frac{\partial c}{\partial x}\right)$, gives the net flux, meaning how many cells are moving in or out of a particular point. The minus sign ensures that cells move towards areas of higher concentration – instead of moving down the gradient, the model needs to reflect how cells move from areas of low chemical concentration to high chemical concentration, hence the minus sign reversing the gradient direction. α is the chemotactic sensitivity, dictating how much influence chemotaxis has on cell movement.

$\frac{\partial c}{\partial t} = -\kappa n$ models how the chemoattractant concentration degrades with the number of cells there are. Biologically, as more cells start to appear at the wound, the concentration of the chemicals decreases in order to signal that there is a sufficient number of cells at the wounded site. $-\kappa n$ models this process, as the larger n becomes, the smaller $\frac{\partial c}{\partial t}$ becomes, until it is eventually depleted.

Similar to the approach taken in the Fisher-KPP equation, we numerically simulated this system of PDEs by considering a discretized rectangular domain Ω, size $N = 100$ by 100, representing a bird's eye view of the wound. We computed the Laplacian with the five-point stencil and implemented Explicit Euler's method.

In order to numerically compute the chemotaxis term $\frac{\partial}{\partial x}\left(\frac{n}{c}\frac{\partial c}{\partial x}\right)$, we first expanded it using the product rule: $\frac{\partial}{\partial x}(\frac{n}{c})\frac{\partial c}{\partial x} + \frac{\partial^2 c}{\partial x^2}\frac{n}{c}$. Using the `np.gradient` function of the `NumPy` library, we computed the spatial gradient of $\frac{n}{c}$, $\frac{\partial}{\partial x}\frac{n}{c}$, as well as the gradient of c, $\frac{\partial c}{\partial x}$, and then computed their dot product. We utilized the five-point stencil to calculate $\frac{\partial^2}{\partial x^2}\frac{n}{c}$, and finally added $\frac{\partial}{\partial x}\frac{n}{c}\cdot\frac{\partial c}{\partial x}$ to $\frac{\partial^2}{\partial x^2}\frac{n}{c}$ (Appendix 1).

We can analyze the influence of parameters α and κ on the evolution of a wound healing. For simplicity, in all of the simulations we keep $r = 0.1$ and $D = 0.05$ constant.

We begin by observing $\alpha = 0.1$ and $\kappa = 0.05$ (Figure 7).

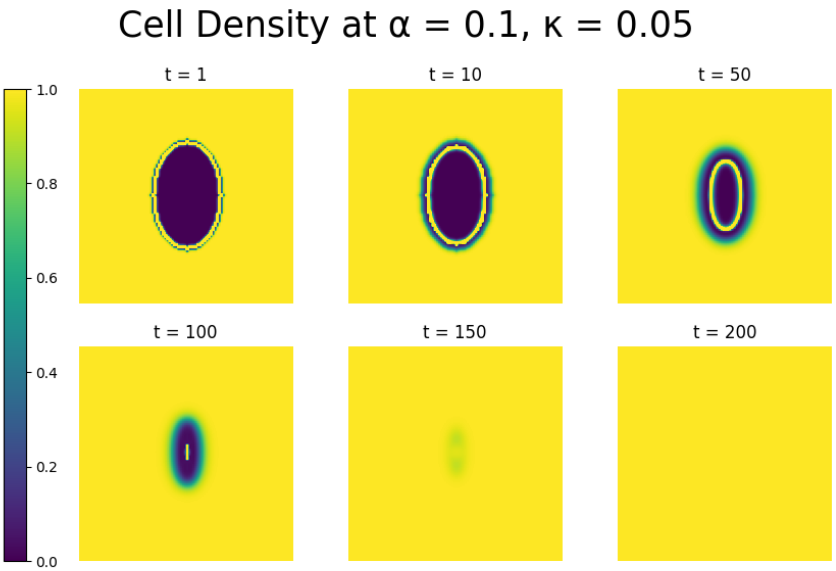

Figure 7: Evolution of the cell density in a wound at different time points following the Keller-Segel model, with $\alpha = 0.1, \kappa = 0.05$.

Figure 7 highlights a key difference between the Fisher-KPP model and the Keller-Segel model: when the chemotaxis term is added, a high-density inner ring of cells forms and migrates towards the wound center. In Figure 8, we observe the chemical concentration $c(x,t)$, and we see how the ring seen in Figure 7 "wraps around" the area of high chemical concentration. The reason for the ring following the chemical concentration stems form the chemotaxis term. At $t = 0$, when the wound is formed, the chemical concentration is set to 1 inside of the wound. Because cells move up this chemical gradient, they accumulate at the wound edge where the gradient is the steepest; this leads to a ring of cells being formed at the edge of the wound. As the time progresses and the cells consume the chemical, the area of high chemical concentration shrinks. The ring of cells follows this gradient inwards, and hence the ring appears to shrink and gradually move towards the center. When the inner ring reaches the center of the cell, meaning the chemical has been completely depleted, these cells being to spread outward due to the growth term $f(n) = 0.1n(1-n)$. Together with the cells outside of the wound migrating inwards, the gap is closed and the wound is healed.

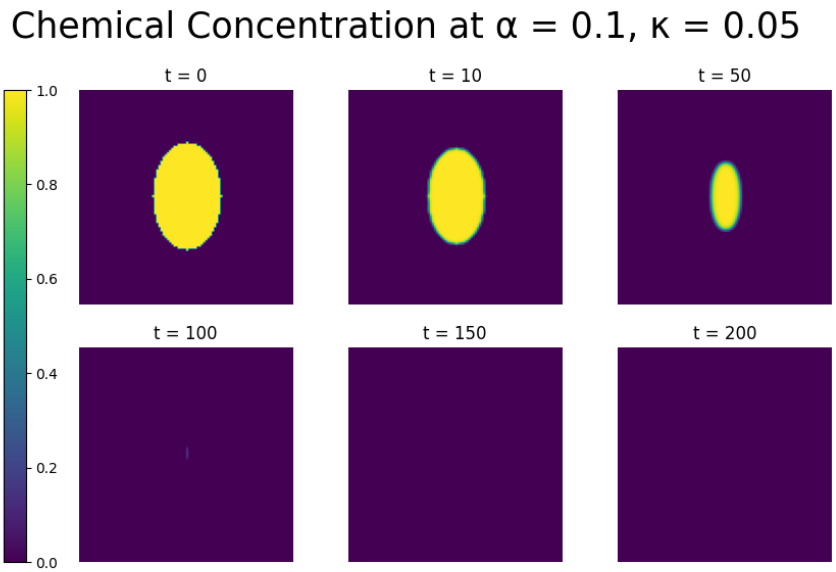

Figure 8: Evolution of the chemical concentration associated to the wound depicted in Figure 7.

Even if we begin with a different wound shape, we still observe this inner ring forming, indicating that chemotaxis really drives cells to respond to their local chemical gradients (Figure 9).

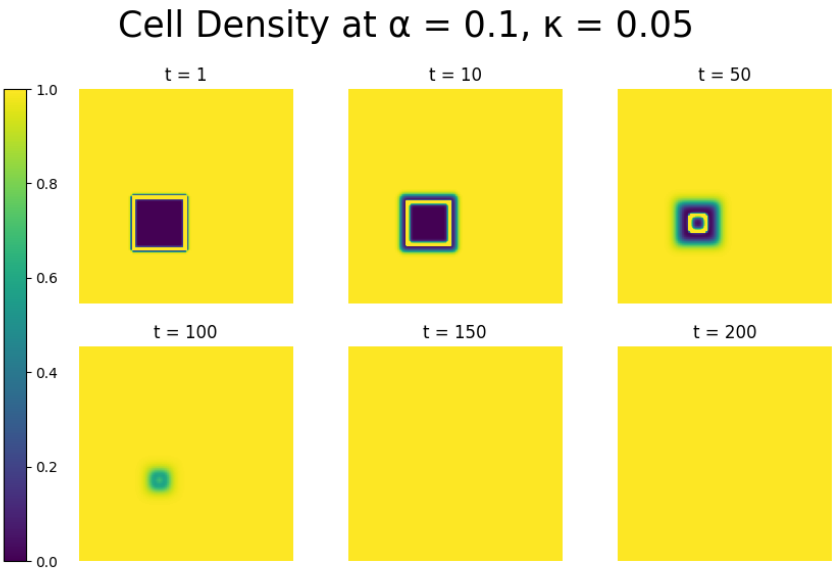

Figure 9: Evolution of the cell density of a rectangular wound, with $\alpha = 0.1, \kappa = 0.05$.

These results are actually consistent with experimental data; soon after the wound is formed, mitotic activity increases in a band (analogous to a ring) near the wound edge, providing an additional population of cells at this source [7]. Previous studies have shown that the greatest mitotic activity occurs at the wound edge, where it can be up to 15 times the rate in normal skin [3]. The agreement between the numerical simulations and the experimental data highlights a key advantage of these mathematical models: they allow the simulation of the effect of various combinations of parameter values on artificial wound healing, without needing to conduct multiple physical experiments.

The α parameter dictates the influence of chemotaxis on the movement of cells. If we decrease α, we expect the wound to close more slowly and the chemical to deplete less quickly, as the movement becomes more diffusion driven. This slowed-down healing is presented in Figure 10 and Figure 11.

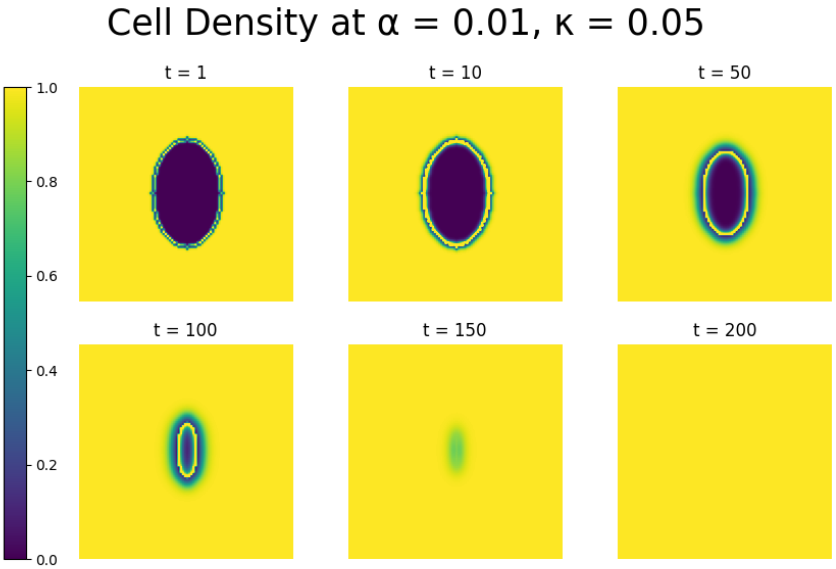

Figure 10: Evolution of the cell density of a wound, with $\alpha = 0.01$, $\kappa = 0.05$.

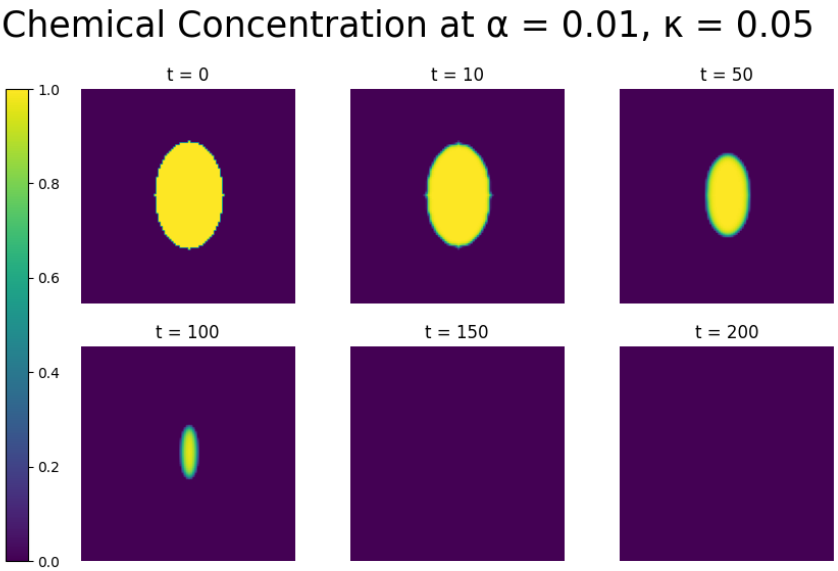

Figure 11: Evolution of the chemical concentration of a wound, with $\alpha = 0.01$, $\kappa = 0.05$.

Intuitively, increasing α would have the opposite effect, where movement becomes more chemotaxis driven and cells therefore move more rapidly towards the wound areas where the chemical gradient is steep. We would expect the inner ring to close faster and consequently the wound to heal quicker.

κ controls the rate at which the chemical degrades in response to the cell density n. Increasing κ means the chemical degrades faster; cells will therefore initially move towards the inside of the wound at a more rapid rate. Nonetheless, once the chemical is depleted, cell movement relies entirely on diffusion, hence the diffusion coefficient D becomes responsible in determining the ability of wound closure. In Figure 12, we can observe that at $t = 100$, the chemical concentration is 0 everywhere as the chemical has already been fully consumed by the cells. In Figure 13, we notice that the inner ring has disappeared, indicating that wound closure is occurring fully based on diffusion and cell growth.

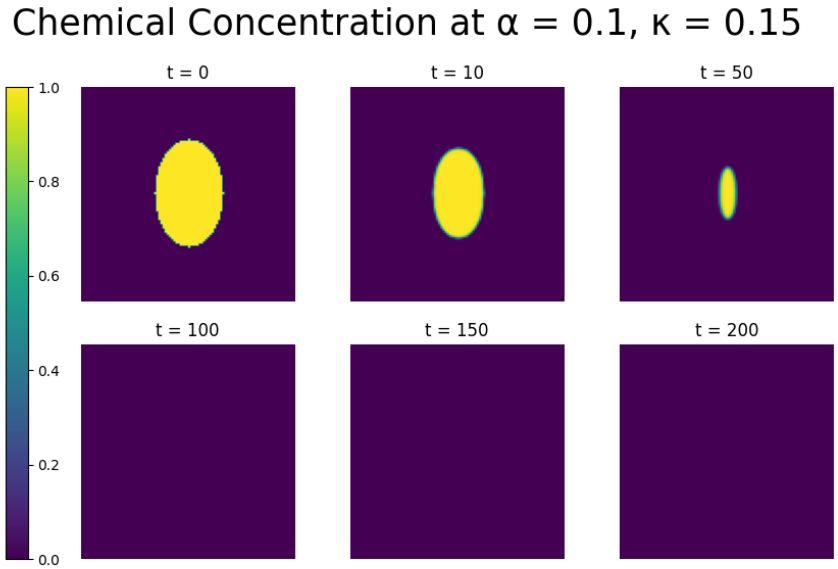

Figure 12: Evolution of the chemical concentration of a wound, with $\alpha = 0.1$, $\kappa = 0.15$.

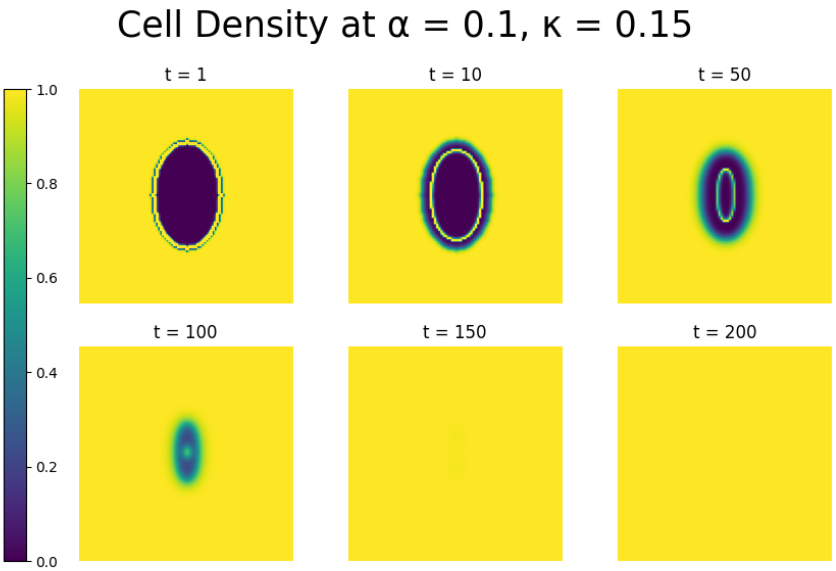

Figure 13: Evolution of the cell density of a wound, with $\alpha = 0.1$, $\kappa = 0.15$.

On the other hand, decreasing κ slows down the degradation of the chemical, meaning the chemical remains in the wound for longer. The inner ring of cells which we have previously observed would remain visible for longer, indicating that wound closure would rely more on chemotaxis driven by the chemical gradient, rather than diffusion of cells alone.

3.1 Chemotaxis with Diffusion

One key limitation of the chemotaxis model presented above is that it lacks a diffusion term for the chemical [5]. In reality, the chemical naturally diffuses throughout the wound area rather than remaining fixed and being depleted only by the cells [3].

For this reason, we can adapt the Keller-Segel model to include a chemical diffusion term:

$$\begin{aligned} \frac{\partial n}{\partial t} &= D\frac{\partial^2 n}{\partial x^2} - \alpha\frac{\partial}{\partial x}\left(\frac{n}{c}\frac{\partial c}{\partial x}\right) + rn(1-n) \\ \frac{\partial c}{\partial t} &= D_c\frac{\partial^2 c}{\partial x^2} - \kappa n \end{aligned} \tag{3}$$

where D_c is now the coefficient of chemical diffusion. The system has now become a reaction-diffusion system of PDEs.

Implementing the same numerical simulation scheme as above with an added Laplacian term to the $\frac{\partial c}{\partial t}$ expression, we explore how perturbing different parameters impacts the pattern formation in the wound.

Firstly, we observe a "baseline" case with $D = 0.15,\ D_c = 0.13,\ \alpha = 0.1,\ r = 0.1$, and $\kappa = 0.01$ (Figure 14, Figure 15). We again observe the same ring forming on the inside of the wound, except this time the ring is much thicker than we had observed in previous figures. The thickness of the ring can be attributed to the chemical diffusion term we added. Diffusion causes the chemical to spread over the wound area, rather than remaining a localized cluster. Cells therefore respond to the chemical gradient in a more spread out way, leading to a thicker band of increased cell activity near the wound edge.

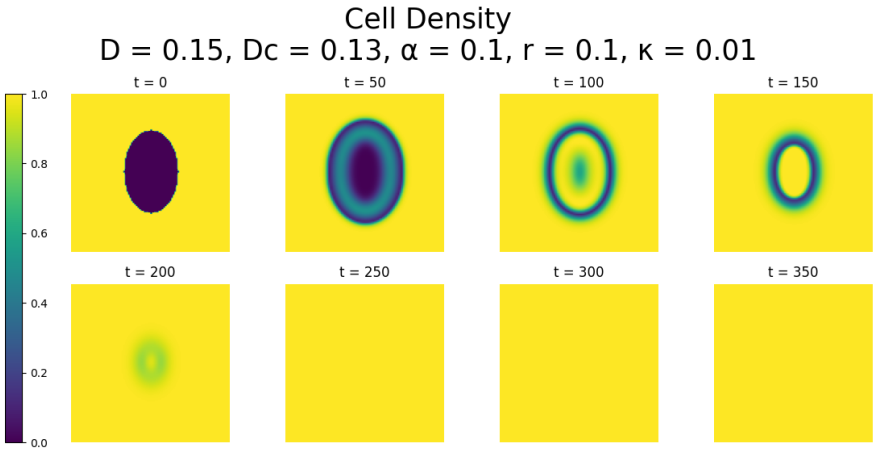

Figure 14: Evolution of the cell density of a wound over 8 discrete time points.

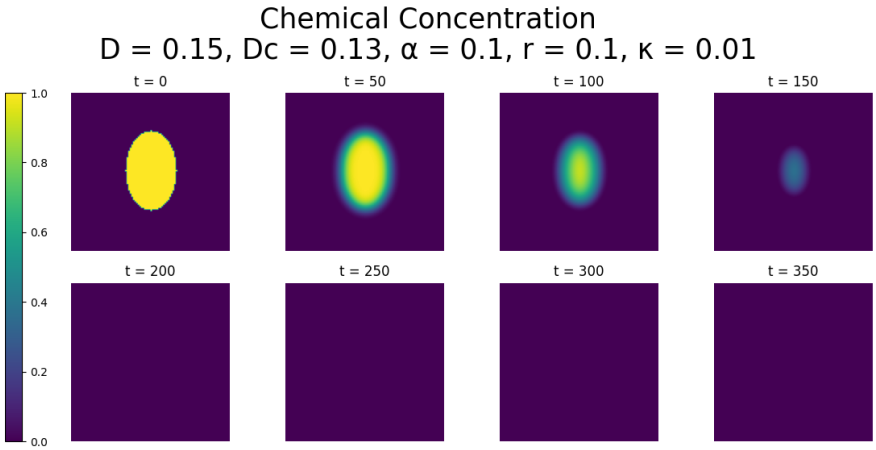

Figure 15: Evolution of the chemical concentration of a wound over 8 discrete time points.

More interesting behaviour appears when we change the diffusion coefficient to $D = 0.3$.

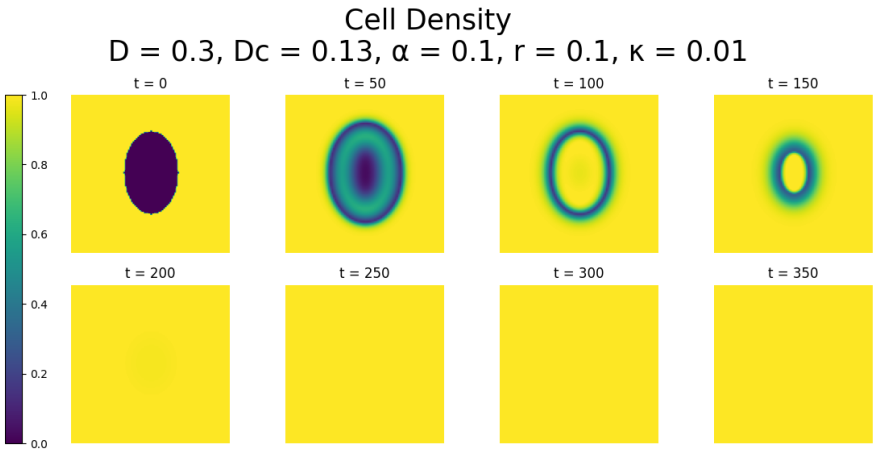

Figure 16: Evolution of the cell density of a wound over 8 discrete time points.

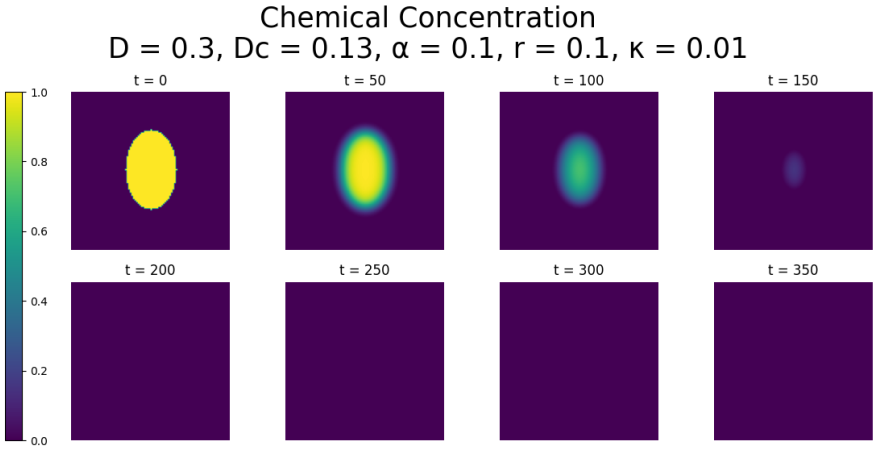

Figure 17: Evolution of the chemical concentration of a wound over 8 discrete time points.

Increasing the cell diffusion coefficient means cells are more motile. In Figure 16, at $t = 100$ the inner ring of high cell density seen in previous figures now appears to be a filled oval area. Because the cells now diffuse more, they are better able cluster more towards the chemical-concentrated area, changing the ring shape into a solid oval.

We can also observe the effect of increasing D_c to 0.25 (Figure 18). D_c is the chemical diffusion coefficient. When D_c is low compared to D, as explored in Figures 16 and 17, the chemical tends to concentrate in an area, and cells gather tightly around this area as it remains quite localized throughout time. Increasing the chemical diffusion coefficient allows the chemical to spread out over space; cells no longer cluster as tightly around the chemical area's edge as this edge has become fuzzier (Figure 19). Therefore, the ring structure forms again.

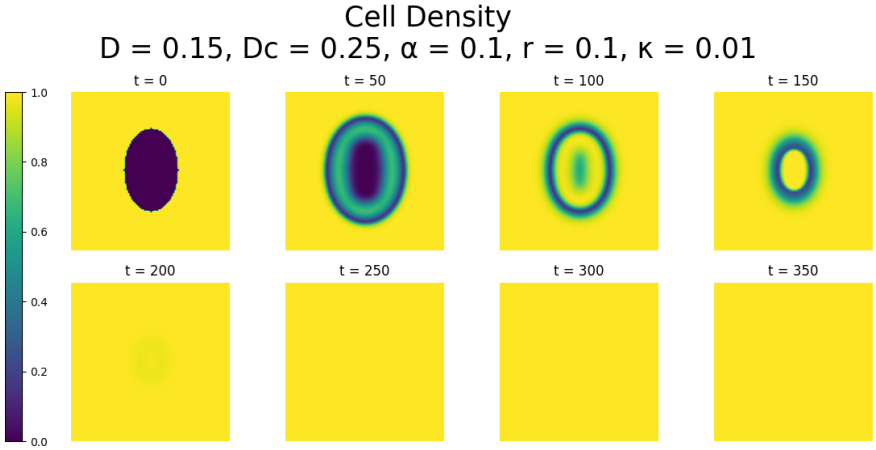

Figure 18: Evolution of the cell density of a wound over 8 discrete time points.

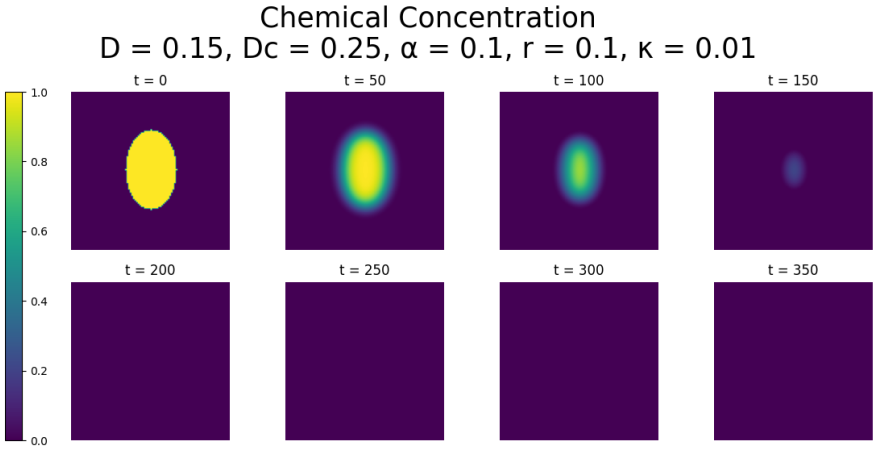

Figure 19: Evolution of the chemical concentration of a wound over 8 discrete time points.

A very extensive range of spatial patterns could be explored with the tuning of these parameters; the full animations are available in Appendix 1. Again, the ability to perturb parameters and observe the effect on an artificial wound highlights the usefulness of these models in replicating experiments in a non-physical and potentially less harmful manner.

4 Advection

Another key biological process involved in wound healing is cell-cell adhesion: the attachment of one cell to another via adhesion molecules. In wound healing, adhesion pulls cells closer together as they migrate to the wound [8]. Cell-cell adhesion can be modeled using an advection term. While both diffusion and advection describe cell transport, diffusion takes into account random cell motion, while advection models directed cell movement.

One model that takes into account nonlocal advection was developed by Armstrong, Painter, and Sherrat:

$$\frac{\partial n(x,t)}{\partial t} = D\frac{\partial^2 n(x,t)}{\partial x^2} - \frac{\partial}{\partial x}\left(n(x,t)\int_{-\rho}^{\rho} g(n(x+\hat{x},t))h(\hat{x})d\hat{x}\right) + f(n(x,t)) \tag{4}$$

Here, $n(x,t)$ represents the one-dimensional continuum density of cells. However, compared to the Fisher-KPP and Keller-Segel models, the initial condition of this advection model is no longer a bird's-eye view of the wound, but rather represents a lateral perspective. $n(x,t)$ therefore measures the depth of the wound at the spatial position x at time t. Moreover, n is no longer bounded between 0 and 1: $n < 1$ still implies that the wound has not healed yet, but $n > 1$ implies there is a local over-concentration of cells present, which can occur as cells "pile up" as adhesion brings them together.

D again represents the diffusion coefficient, $\frac{\partial^2}{\partial x^2}$ is the one-dimensional Laplacian operator in Cartesian coordinates, and $f(n(x,t))$ is the cell growth, modeled by the same logistic growth equation $n(1-n)$.

Nonlocal advection is modeled by the $-\frac{\partial}{\partial x}\left(n(x,t)\int_{-\rho}^{\rho} g(n(x+\hat{x},t))h(\hat{x})d\hat{x}\right)$ term. Here, we introduce a new variable $\hat{x}$, representing the displacement from any given position x. By integrating with respect to the displacement $\hat{x}$, in the integral $\int_{-\rho}^{\rho} g(n(x+\hat{x},t))h(\hat{x})d\hat{x}$ we consider all of the cells in a circular region of radius ρ, centered at position x. This integral is therefore a nonlocal integral, as it depends on x as well as cells surrounding x.
$g(n(x+\hat{x},t))$ models the strength of the adhesive force exerted on cells at position x by neighboring cells at positions $x+\hat{x}$. g is a function of n, which is itself a function of x and $\hat{x}$. These dependencies represent how the strength of the adhesive force depends on the cell density present in a region around x. If there are no cells in the region around x, then the adhesive force must be zero: $g(0) = 0$. If there are some cells, $g(n) > 0$ [9]. However, if there are too many cells in the neighboring area, the adhesive force decreases – the cell environment becomes more rigid as the space between cells diminishes due to overcrowding, making it harder for cells to access other cells' adhesion molecules [10]. Therefore, this model sets $g(n) = n(\lambda - n)$, where λ is the cell-cell adhesion constant. This is a concave parabola in n with roots at $n = 0$ and $n = \lambda$. Obviously, $g(0) = 0$. When $n \in (0, \lambda)$, $g(n) > 0$, and therefore cells attract each other. However, if $n > \lambda$, $g(n) < 0$: adhesion becomes repulsive, causing cells to move away from each other to avoid overcrowding (Figure 20).

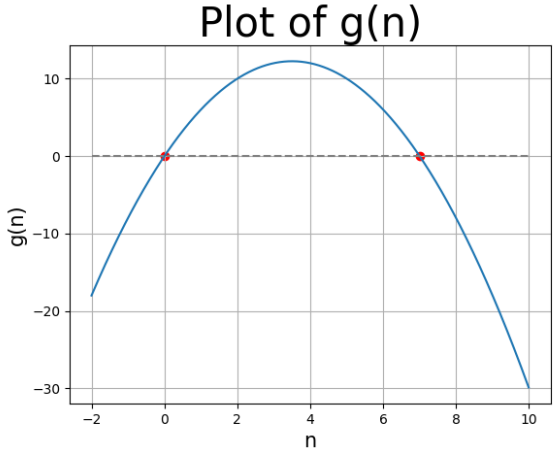

Figure 20: Plot showing the general shape of $g(n)$. Here, λ is set to 7.

$h(\hat{x})$ represents the direction and magnitude of the cell-cell adhesive forces acting on cells at position x, due to neighboring cells at position $x + \hat{x}$. h depends purely on the displacement $\hat{x}$, as it models a purely mechanical pulling process:

- If the displacement $\hat{x} > 0$, the neighboring cells are to the right of the cells at x; the adhesive force pulls the cells at position x to the right, and therefore $h(\hat{x}) > 0$.
- If $\hat{x} < 0$, the neighboring cells are to the left of the cells at x; the adhesive force pulls the cells at position x to the left, and therefore $h(\hat{x}) < 0$.

We also require the derivative of $h(\hat{x})$ to approach 0 the further away cells $x+\hat{x}$ are from x, as this reflects the biological assumption that distant cells exert less force on the cell at x. In the model, we set $h(\hat{x}) = \frac{0.1 \arctan(0.1\hat{x})}{\arctan(2.0)}$, as it is odd, bounded, and its derivative approaches 0 as $\hat{x} \to \pm\infty$ (Figure 21).

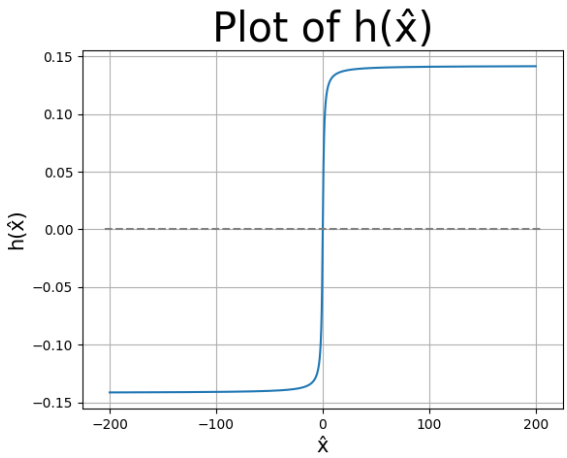

Figure 21: Plot of $h(\hat{x})$ over the spatial domain.

Therefore, $h(\hat{x})$ and $g(n(x+\hat{x},t)$ play related yet distinct roles in modeling advection. $g(n(x+\hat{x},t)$ represents how strongly neighboring cells pull the cells at x towards them, whereas $h(\hat{x})$ highlights the direction that this pulling motion occurs at and ensures that cells distant from x do not have the same adhesive force as cells closer to x. Essentially, $g(n(x+\hat{x},t))$ considers the number of cells at $x+\hat{x}$ while $h(\hat{x})$ considers how far these cells are from x.

When we take the product of $g(n(x+\hat{x},t))$ with $h(\hat{x})$, we are representing the signed adhesive force that cells at $x+\hat{x}$ have on cells at x. Integrating this product, $\int_{-\rho}^{\rho} g(n(x+\hat{x},t))h(\hat{x})d\hat{x}$, we represent the net adhesive force that acts on the cells at position x from all neighboring cells within the sensing radius ρ. In simple terms, this is a weighted average of how much the neighbors of cell x affect its movement.

We proceed by multiplying this integral by $n(x,t)$, the cell density at x. This is to account for the fact that only cells present at position x are able to respond to the adhesive force; intuitively, if there are no cells at x, then no cells are able to respond to the adhesive force $\int_{-\rho}^{\rho} g(n(x+\hat{x},t))h(\hat{x})d\hat{x}$, whereas if there is a high cell density at x, more cells are available to respond and therefore more will flow.

Finally, we take the partial derivative with respect to the spatial variable x of the expression $n(x,t)\int_{-\rho}^{\rho} n(x+\hat{x},t)(\lambda - n(x+\hat{x},t))\frac{0.1\arctan(0.1\hat{x})}{\arctan(2.0)}d\hat{x}$. This ensures we look at how the adhesive flux changes over space, and essentially how the movement of cells because of adhesion changes from one location to another. If the adhesive flux increases at x, the cell density is decreasing at x, hence we must subtract this derivative from $\frac{\partial n(x,t)}{\partial t}$.

Substituting the $g(n(x+\hat{x},t))$ and $h(\hat{x})$ functions into Equation 4, we obtain the following

complete advection model [9]:

$$\frac{\partial n(x,t)}{\partial t} = D\frac{\partial^2 n}{\partial x^2} - \frac{\partial}{\partial x}\left(n(x,t)\int_{-\rho}^{\rho} n(x+\hat{x},t)(\lambda - n(x+\hat{x},t))\frac{0.1\arctan(0.1\hat{x})}{\arctan(2.0)}d\hat{x}\right) + n(1-n) \tag{5}$$

To numerically simulate this equation, we begin by discretizing the spatial domain, considering a one-dimensional region $L \in [-200, 200]$. We compute the diffusion term $D\frac{\partial^2 n}{\partial x^2}$ with the five-point stencil of the Laplacian.

For every x in the spatial domain, we must compute the integral $\int_{-\rho}^{\rho} n(x+\hat{x},t)(\lambda - n(x+\hat{x},t))\frac{0.1\arctan(0.1\hat{x})}{\arctan(2.0)}d\hat{x}$. The number of spatial points in the discretization is dependent on the spatial step dx: $N = \frac{L}{dx}$. We therefore have arrays $\mathbf{x}$ and $\mathbf{n}$ of length $\frac{L}{dx}$. When we integrate with respect to $\hat{x}$, we consider the cells at positions $[x-\rho, r+\rho]$, and therefore in these arrays we consider the indices $[x - \frac{\rho}{dx}, x + \frac{\rho}{dx}]$.

In order to calculate the integral for every x, we utilize a for-loop. $h(\hat{x})$ can be calculated outside of this loop as it depends purely on displacement and remains the same for every x position we consider. Outside the loop, we also compute $g(n)$ for every value of n. Inside the loop, we index $g(n)$ at the appropriate neighbors by considering $\frac{\rho}{dx}$ values to the left and to the right of x. We then take the product of $h(\hat{x})$ with the indexed neighbors of x, and approximate the integral using the trapezoidal rule.

We multiply the array of integrated values with the array of cell densities $\mathbf{n}$, and compute the partial derivative with respect to x of this expression using a finite difference approximation.

We define the PDE by adding the Laplacian, the advection term, and the growth term $\mathbf{n}(\lambda - \mathbf{n})$, and then use Explicit Euler's method to evolve the system over time.

We can test the influence of the parameters λ and ρ on whether a wound heals or not.

We begin by observing $\lambda = 5, \rho = 17$ (Figure 22).

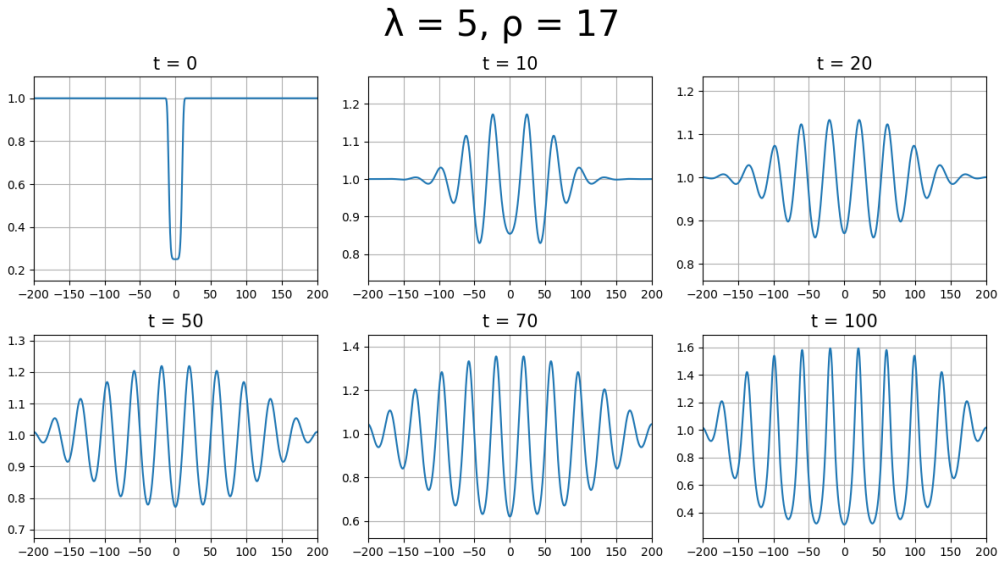

Figure 22: Wound healing evolution with $\lambda = 5$ and $\rho = 17$.

As the wound begins to heal, waveforms appear. This is due to the advection term, as it creates areas of higher cell density and areas of lower cell density. The amplitude of these oscillations is what determines whether a wound has healed or not. If a wound is healing, we expect the amplitudes to be decreasing with time, reaching the spatially homogeneous steady state $n(x,t) = 1$; if a wound is unable to heal, the amplitudes will keep increasing. Here, at $t = 100$ the waves have amplitudes up to 1.6. This indicates that with this particular combination of parameter values, the system is unstable as adhesion causes over-clustering of cells, preventing the wound from healing.

However, if we decrease ρ to 16, the system stabilizes and the wound heals, as seen in Figure 23. As the wound healing process begins ($t > 0$), waves start to grow, but their amplitude decreases with time. At $t = 100$, the maximum amplitude is around 1.05, indicating that the solution is converging to the homogeneous steady state $n(x, t) = 1$. Decreasing ρ decreases the sensing radius around each cell x, meaning that cells interact more locally with each other. This prevents very large clusters from forming, allowing cells to keep diffusing towards the area of lower concentration and therefore aid in closing the wound.

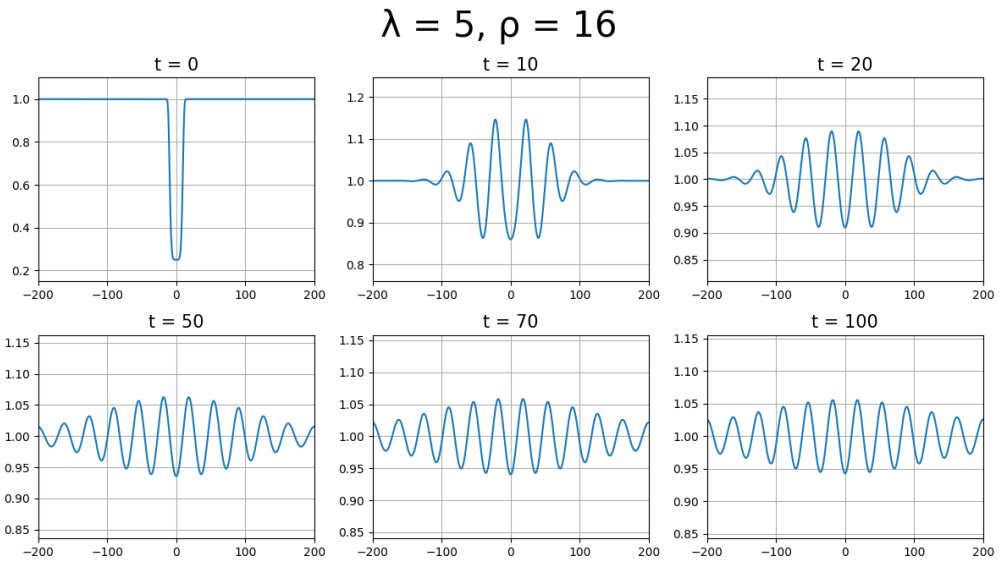

Figure 23: Wound healing evolution with $\lambda = 5$ and $\rho = 16$.

Decreasing λ has a similar effect to decreasing ρ. In Figure 24, we set $\lambda = 4$ and $\rho = 17$.

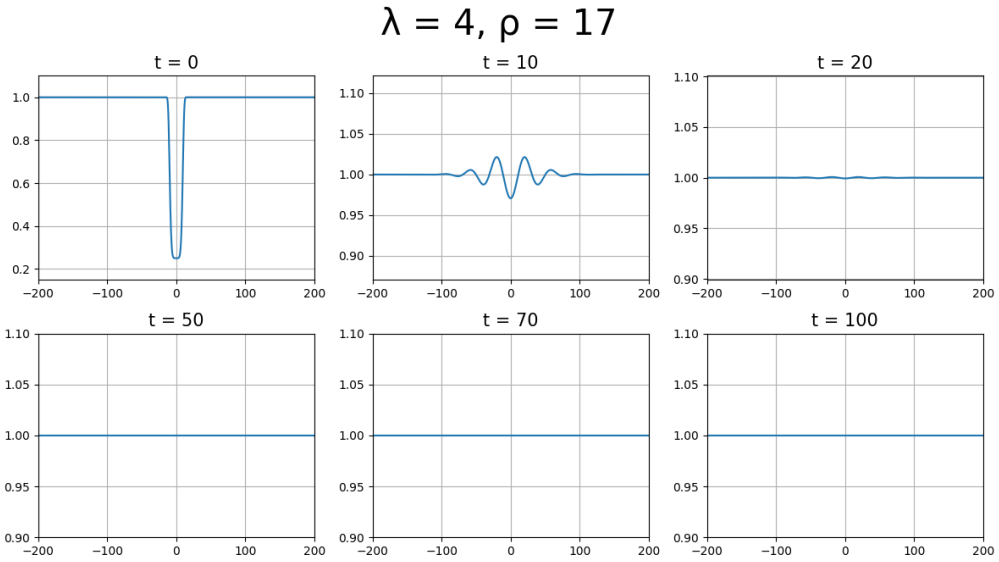

Figure 24: Wound healing evolution with $\lambda = 4$ and $\rho = 17$.

We can observe how oscillations completely flatten by $t = 100$ and the system reaches the homogeneously stable solution $n(x, t) = 1$. λ dictates the strength of the cell-cell adhesion; with

a lower value of λ, cells are less attracted to each other which prevents localized clusters from forming, allowing cells to more smoothly travel to the wound edge.

This naturally begs the question of why biological systems have these adhesive forces, if this model shows that the lower the adhesion is, the faster the wound heals.

Biologically, cell-cell adhesion is essential as it is what maintains a tissue intact, holding the epithelial cells together and preventing the tissue from disintegrating into individual cells [11]. Even though adhesion appears to slow down the wound healing process, it is necessary to ensure that cells migrate as tissues rather than individual units.

The process of wound healing is very complex, and boiling it down to one partial differential equation is bound to require simplifications. One key simplification this model makes is ignoring what occurs when adhesion is too little. In a real wound, cell-cell adhesion is regulated by many chemical pathways. As the wound healing process begins, the adhesive force is reduced to make sure cells are able to travel to areas of lower cell density instead of being overly attracted to each other and forming localized clusters. Then, towards the end of the process, adhesion increases again to make sure the tissues are well connected [12]. This advection model is unable to capture this process, and therefore it appears that with minimal adhesion the wound heals perfectly.

This highlights an essential limitation in many mathematical models of wound healing. Although they can provide useful information into certain aspects of the wound healing process, the insights they provide are isolated to specific behaviours. Creating a model that encapsulates the wide range of processes involved in wound healing is difficult, but isolating these behaviours into single models introduces inconsistencies due to the interconnectedness of these processes.

5 Conclusion

This project explored several mathematical models that attempt to describe various aspects of wound healing: the Fisher-KPP model for simple diffusion and growth, the Keller-Segel model incorporating chemotaxis, an extension of the Keller-Segel model taking into account the diffusion of the chemical, and an advection-centered model focused on cell-cell adhesion.

The models explored in this paper are just a few of the many that have been developed over the past decades to try to describe wound healing. Wound healing is, like many other biological processes, dominated by the interaction between various cells, molecules, proteins, and chemicals. These inter-dependencies make it difficult to create a model which is perfectly able to isolate and model just one of the aspects of wound healing.

For example, while the Fisher-KPP provides great insight into how diffusion and growth can impact whether a wound heals or not, it ignores key aspects of wound healing such as chemical regulations of cell movement. Moreover, while the Keller-Segel model models how cell movement is stimulated by a chemical, in a real wound there is not just one chemical that regulates the cell movement. Multiple chemicals, each with a different function, are present, and the Keller-Segel model is a great simplification of this complex process.

Many assumptions are also made in these models in order to simplify the modeling process. For example, in the Keller-Segel model, the chemical concentration is initially assumed to be 1 inside the entire wound. While this simplifies the calculations required in the model, it is unrealistic, as the cells produce the chemical and therefore it makes little biological sense that once a wound is formed the chemical is already present at its highest possible density. A more biologically accurate model would take into account the different types of cells near a wound, differentiating between the ones that produce the chemicals and the ones that migrate inwards to aid in healing. We therefore observe a key tradeoff in these models: we must sacrifice simplicity in order to obtain more biological accuracy.

Nonetheless, despite their limitations, having models with the ability to tune parameters can be useful to simulate certain experimental conditions. One can base the parameter values on observed experimental data, and perform perturbations to these to observe how the system would react to different conditions, This is particularly useful in the wound healing context where conducting experiments could be unethical due to undue stress or harm.

Ultimately, the field of mathematical models of wound healing is still evolving, as models are continuously being developed to try to capture more of the biological complexity in the healing process. Despite the many limitations of the existing models, they are able to give insights into some of the underlying mechanisms in wound healing and somewhat offer a framework for identifying how different factors influence whether a wound heals or not.

References

[1] Jorgensen, Stephanie N., and Jonathan R. Sanders. "Mathematical models of wound healing and closure: A comprehensive review." Med Biol Eng Comput, vol. 54, no. 9, 30 Dec. 2015, pp. 1297–1316, https://doi.org/10.1007/s11517-015-1435-z.

[2] Werner, Sabine, and Richard Grose. "Regulation of wound healing by growth factors and cytokines." Physiological Reviews, vol. 83, no. 3, 1 July 2003, pp. 835–870, https://doi.org/10.1152/physrev.2003.83.3.835.

[3] Murray, James Dickson. "Epidermal Wound Healing." *Mathematical Biology II: Spatial Models and Biomedical Applications*, 3rd ed., vol. 18, Springer, 2003, pp. 441–482.

[4] Habbal, Abderrahmane, et al. "Assessing the ability of the 2D Fisher–KPP equation to model cell-sheet wound closure." Mathematical Biosciences, vol. 252, 3 Jan. 2014, pp. 45–59, https://doi.org/10.1016/j.mbs.2014.03.009.

[5] Hulzebos, Jessica Ann. *Keller-Segel models for chemotaxis*. 2017. Iowa State Univeristy, Master's Thesis. https://faculty.sites.iastate.edu/jyan/files/inline-files/Hulzebos-thesis.pdf.

[6] Lakhani, Vinal, and Timothy C. Elston. "Testing the limits of Gradient Sensing." PLOS Computational Biology, vol. 13, no. 2, 16 Feb. 2017, https://doi.org/10.1371/journal.pcbi.1005386.

[7] Bereiter-Hahn, Jürgen. "Epidermal cell migration and wound repair." Biology of the Integument, 1986, pp. 443–471, https://doi.org/10.1007/978-3-662-00989-5_23.

[8] "Gene Ontology Browser." Cell-Cell Adhesion Gene Ontology Term, www.informatics.jax.org/vocab/gene_ontology/GO:0098609. Accessed 11 May 2025.

[9] Webb, Glenn. "The force of cell-cell adhesion in determining the outcome in a nonlocal advection diffusion model of wound healing." Mathematical biosciences and engineering : MBE vol. 19,9 (2022): 8689-8704. doi:10.3934/mbe.2022403

[10] Selhuber-Unkel, C., et al. "Cell adhesion strength is controlled by intermolecular spacing of adhesion receptors." Biophysical Journal, vol. 98, no. 4, Feb. 2010, pp. 543–551, https://doi.org/10.1016/j.bpj.2009.11.001.

[11] Gumbiner, Barry M. "Cell adhesion: The molecular basis of tissue architecture and morphogenesis." Cell, vol. 84, no. 3, Feb. 1996, pp. 345–357, https://doi.org/10.1016/s0092-8674(00)81279-9.

[12] Koivisto, Leeni, et al. "Integrins in wound healing." Advances in Wound Care, vol. 3, no. 12, Dec. 2014, pp. 762–783, https://doi.org/10.1089/wound.2013.0436.

6 Appendix

The code used in the simulations can be found here.